Numerical modelling of chromatic effects on axicon-focused beams used to generate HOFI plasma channels

Journal of Physics: Conference Series **1596** (2020) 012049 doi:10.1088/1742-6596/1596/1/012049

Numerical modelling of chromatic effects on axicon-focused beams used to generate HOFI plasma channels

A J Ross, A Alejo, A von Boetticher, J Cowley, J Holloway, J Jonnerby, A Picksley, R Walczak and S M Hooker

John Adams Institute for Accelerator Science and Department of Physics, University of Oxford, Denys Wilkinson Building, Keble Road, Oxford, OX1 3RH, UK

E-mail: aimee.ross@physics.ox.ac.uk

Abstract. Hydrodynamic optical-field-ionised (HOFI) plasma channels promise a route towards high repetition-rate, metre-scale stages for future laser plasma accelerators. These channels are formed by hydrodynamic expansion of a plasma column produced by optical field ionisation at the focus of a laser, typically from an axicon lens. Since the laser pulses used to generate the initial plasma column are of sub-picosecond duration, chromatic effects in the axicon lens could be important. In this paper we assess these effects using a numerical propagation code. The code is validated using analytical formulae and experimental data. For the parameter range investigated, dispersive effects are found to be of minor importance, reducing the peak on-axis intensity in the focal region by approximately 10%.

1. Introduction

The ability of laser wakefield accelerators (LWFAs) to generate GeV electron beams in centimetre distances makes them interesting for applications in high-energy physics, imaging, industry, and medicine [1]. To reach multi-GeV energies in a single LWFA stage, low plasma densities ($\sim 10^{17}\,\mathrm{cm}^{-3}$), and long acceleration lengths ($\sim 100\,\mathrm{mm}$), are required [2]. Due to diffraction, the drive laser would not ordinarily remain focused over these distances, limiting the acceleration length. The laser pulse must therefore be guided, either by self-guiding [3] or using a separate waveguide structure. The latter has a number of advantages, such as being independent of drive laser power and allowing the plasma accelerator to operate in the quasi-linear regime as opposed to the bubble regime, which can bring greater control of electron injection and acceleration [4].

Guiding of high-intensity laser pulses in gas filled capillary-discharge waveguides has been achieved over distances of several centimetres [5–7]. However, these structures are prone to laser damage due to pointing fluctuations of the laser. For future laser plasma accelerators operating at higher repetition rates, it would be preferable to use free-standing, all-optical plasma channels. For these channels, a laser pulse arrives ahead of the main drive laser, ionises the gas and heats the plasma. The hot plasma column expands rapidly into the cold surrounding gas, driving a radially expanding shock front. The resulting plasma density profile forms a gradient-index waveguide.

In the original work [8], the initial plasma columns were heated by laser-driven collisions which become ineffective at the low densities of interest for multi-GeV LWFAs. In order to

overcome this difficulty, hydrodynamic optical-field-ionised (HOFI) plasma channels have been developed [9]. In the HOFI scheme, the electrons are liberated with large kinetic energies via optical field ionisation, generating a heating effect which is independent of density. Plasma channels with on-axis densities as low as $1.5 \times 10^{17}\,\mathrm{cm}^{-3}$ and matched spot sizes in the range $20 - 40\,\mu$m have been produced with this approach [10].

In order to maximise the length of the plasma channel, the initial laser pulse is focused to an extended longitudinal region. A number of optics can be used to achieve a line focus, such as axicons [11] and axilenses/axiparabolas [12, 13]. These optics focus the light from different radial positions on the incident laser pulse to different points along the focal line (see Figure 1 for the case of an axicon). To form the plasma channel, the on-axis intensity along the focus must be above the ionisation threshold of the gas species. For optical field ionisation, peak intensities of order $10^{14} - 10^{16}\,\mathrm{Wcm}^{-2}$ are required and hence the pulse duration must be short for the energy of the channel-forming pulse to be kept to a reasonable value. These short pulses have a corresponding broad bandwidth. Hence a full understanding of the operation of the focusing optic must account for chromatic effects.

In this study, we present a numerical code which simulates the propagation of laser pulses through a series of optics, taking into account chromatic effects. The code is described in Section 2 and tested against analytic results and experiment for the case of a monochromatic beam propagating through a single axicon lens. In Section 3, the effects of dispersion through a refractive axicon are modelled using parameters relevant to a recent experiment on the Rutherford Appleton Laboratory Astra-Gemini laser TA2 [10].

2. Numerical Code

2.1. Method

The numerical code developed in this study models the evolution of the field of a laser pulse as it propagates through a sequence of optical elements to an output plane. The initial transverse and longitudinal shape of the pulse is defined in the input script, as well as the optic type and material properties. The incident laser pulse is taken to have a flat spatial phase front unless otherwise stated.

Free space propagation is modelled using the angular spectrum method [14], which assumes only that the scalar wave equation holds. The method involves taking a 2D Fourier transform of the complex transverse field to generate the spectrum in transverse wave-number, or 'angular' space (k_x, k_y). Each point in angular space is then evolved via:

$$\tilde{U}(k_x, k_y; z) = \tilde{U}(k_x, k_y; 0)\mathcal{H}(k_x, k_y, z) \tag{1}$$

where $\mathcal{H}(k_x, k_y, z) = \exp\left(\mathrm{i}\sqrt{k^2 - (k_x^2 + k_y^2)}\; z\right)$ is the propagator function [14] ($k = 2\pi/\lambda$ for wavelength λ). An inverse 2D Fourier transform recovers the output field at the plane z.

Optical elements are modelled by multiplying the incident amplitude by a complex amplitude transmission function which depends on transverse position. Equivalently, the optic can be introduced in the spectral domain via a convolution of the spectral field amplitude with the Fourier transform of the amplitude transmission function. All optics are treated as 'thin', i.e. the total phase accumulated is applied at one z-position and the laser does not evolve within the optic itself.

The process described is valid for monochromatic light, i.e. a continuous wave laser. To understand the behaviour of a broadband, short-pulse laser, it is necessary to model the full spectrum of the pulse. In our code, the spectrum is generated via a Fourier transform of the incident temporal profile and a number of discrete frequencies are sampled. For each frequency, the initial field amplitude is scaled by the spectral shape, for example for a Gaussian spectrum;

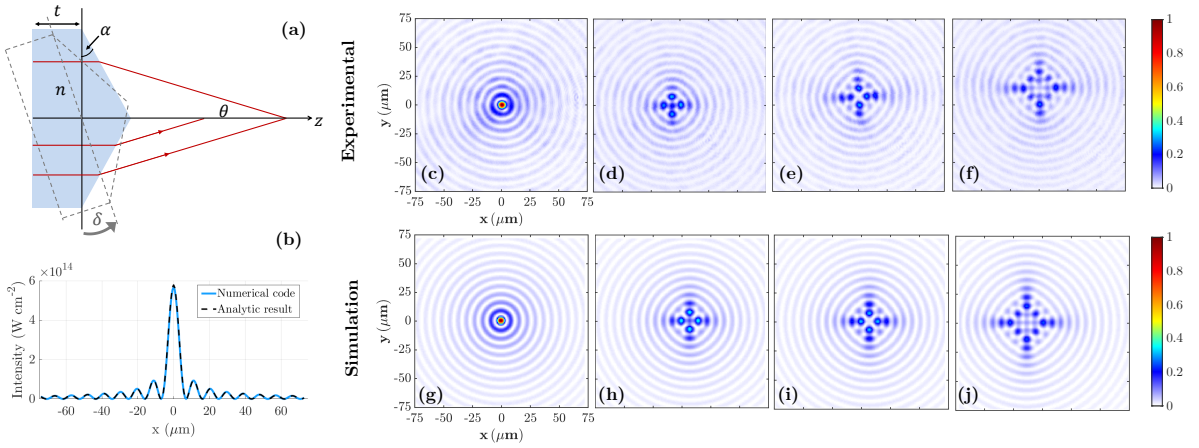

Figure 1. Validation of the code for the case of a refractive axicon as shown in (a), where α is the axicon base angle, t is the substrate thickness, $n(\lambda)$ is the refractive index and θ is the approach angle. In (b), the output of the code is compared to the analytic expression for a single wavelength of 800 nm, at $z = 15$ mm. (c-f) are the focal spots produced for different values of misalignment angle, δ, with (c) being the $\delta = 0.0$ mrad case. These images were found experimentally for $\lambda = 633$ nm at $z = 140 \pm 2$ mm downstream of the axicon, for misalignment angles $\delta = 22.0,\ 33.0,\ 44.0 \pm 0.4$ mrad respectively (d-f). These can be compared to the focal spots generated by the numerical code shown in (g-j) recorded at 140 mm from the axicon, at angles $\delta = 0.0,\ 49.5,\ 55.0,\ 66.0$ mrad. The colour scales in (c-j) are normalised to the peak of (g).

$$U_\omega(x, y, z = 0, \omega) = U(x, y, z = 0) \exp\left[-\frac{(\omega - \omega_0)^2}{2\sigma^2}\right] \tag{2}$$

where $\omega = 2\pi c/\lambda$, ω_0 is the central frequency and σ is the $1/e^2$ bandwidth of the spectral intensity. U_ω then evolves via the steps described above. The field at a particular transverse position in the output plane (x, y) may be extracted for each frequency. The temporal profile may then be retrieved by an inverse Fourier transform;

$$U_t(x, y, z, t) = \mathcal{F}_t^{-1}[U_\omega(x, y, z, \omega)]. \tag{3}$$

The simulation box size and the number of grid points must be chosen so as to be consistent with the desired resolution in the transverse domain, whilst satisfying the Nyquist sampling conditions. In this work, a typical simulation employed a transverse spatial grid of 20000×20000 pixels, covering a transverse spatial extent of 20 mm × 20 mm. Propagation distances were of order 15 mm and a spectral grid of 1000 wavelengths was used. The code was written in MATLAB and run on a personal computer with 256 GB RAM. To reduce running time, the propagation of each wavelength was calculated in parallel, utilising the MATLAB parallel computing capabilities. With these settings, a simulation with a single propagation step of a broadband pulse took approximately 30 minutes to run.

2.2. Code validation

The code was checked for the case of a Gaussian, monochromatic beam propagating through an axicon. An axicon is characterised by a base angle α, substrate thickness t and refractive index $n(\lambda)$ (see Figure 1(a)). The approach angle $\theta \simeq (n - 1)\alpha$ (for small angles) determines the length and radius of the focal line.

The field distribution at a position z after the axicon can be calculated theoretically using the Fresnel approximation and the method of stationary phase [15]. For a Gaussian incident beam of wavelength λ and beam waist w_0, the output field at radius ρ takes the form, following [15];

$$\begin{aligned} U(\rho, z) = -\mathrm{i}CU_0(2\pi kz)^{1/2}(n-1)\alpha \exp(\mathrm{i}\pi/4) \exp(\mathrm{i}kz) \exp[-\mathrm{i}kz(n-1)^2\alpha^2/2] \\ \times \exp(\mathrm{i}k\rho^2/2z) \exp[-z^2(1-n)^2\alpha^2/w_0^2] J_0[(n-1)k\rho\alpha] \end{aligned} \tag{4}$$

where J_0 is the zeroth order Bessel function of the first kind. Here $C = T_1T_2 \exp(\mathrm{i}knt)$ where T_1 and T_2 are the amplitude transmission coefficients for the air-glass and glass-air boundaries, which are approximated as $T_1 \simeq T_2 \simeq 1$. The focal spot size can be defined by the location of the first minimum which occurs at a radius $r_0 = 2.4048/k\theta$.

For this study, the axicon parameters were taken to be $\alpha = 5.52\,^\circ$, $t = 3.0\,\mathrm{mm}$ and the refractive index $n(\lambda)$ was calculated from the Sellmeier equation for fused silica [16]. The transverse intensity profile after the numerical propagation from this axicon is displayed in Figure 1(b). The transverse intensity profiles calculated by the code and Eq. 4 are found to be in agreement.

It is found experimentally that small angular misalignments of the axicon degrade the focal spot quality substantially. This behaviour can be investigated using the numerical code. For the experimental demonstration, the beam from a helium-neon laser, operating at $\lambda = 633\,\mathrm{nm}$, was expanded and propagated through a refractive axicon with the same parameters as above. The axicon focus was imaged by a microscope objective onto a CCD camera at $z = 140 \pm 2\,\mathrm{mm}$ downstream of the axicon.

To set the angle δ (see Figure 1(a)), the axicon alignment was first optimised to give a focus best resembling the ideal Bessel shape. This fixed $\delta = 0.0\,\mathrm{mrad}$. The screw on the axicon mount was then used to introduce small angular offsets and the camera was moved transversely to keep the focal spot on the screen. The angles between the axicon and incident beam were determined by calibrating the screw turns, giving $5.5 \pm 0.4\,\mathrm{mrad}$ per turn, where the error represents the uncertainty on the angle measurement. The spots displayed in Figures 1(d-f) were produced at $\delta = 22.0$, 33.0, and $44.0 \pm 0.4\,\mathrm{mrad}$ respectively.

In the numerical code, the angular misalignments are implemented by applying a tilt to the incident beam before it reaches the axicon. This is equivalent to varying the angle of the axicon with respect to the incident beam as in the experiment. For a tilt about the y-axis, a phase is applied to the incident beam as a function of transverse position x of the form $\phi_\delta = kx\tan(\delta)$. Additional phase introduced by refraction inside the axicon can be estimated geometrically and is found to be negligible for the angles considered here. The laser and axicon parameters in the simulation were chosen to match those in the experiment and δ was varied in steps of 5.5 mrad between 44.0 and 71.5 mrad. The resulting focal spots were compared to the experimental results in Figures 1(d-f) to identify the misalignment angle required in simulation for equivalent spot degradation.

To find the simulated image which most closely corresponds to each of the experimental images, the average root-mean-square (RMS) deviation was calculated between a line-out along the x-axis of the experimental image and the line-outs of the simulated images. The simulated image which gave the minimum average RMS deviation was selected. The best-match simulated images are presented in Figures 1(h-j) and were generated using $\delta = 49.5$, 55.0, and 66.0 mrad respectively, however improved matching may be found for values of δ between the steps used in the simulation.

The smaller values for δ found in the experiment compared to the simulation may be a result of several experimental factors. The spot at $\delta = 0.0\,\mathrm{mrad}$ found experimentally (Figure 1(g)) does not have perfect azimuthal symmetry. This is likely a sign of other aberrations in the near

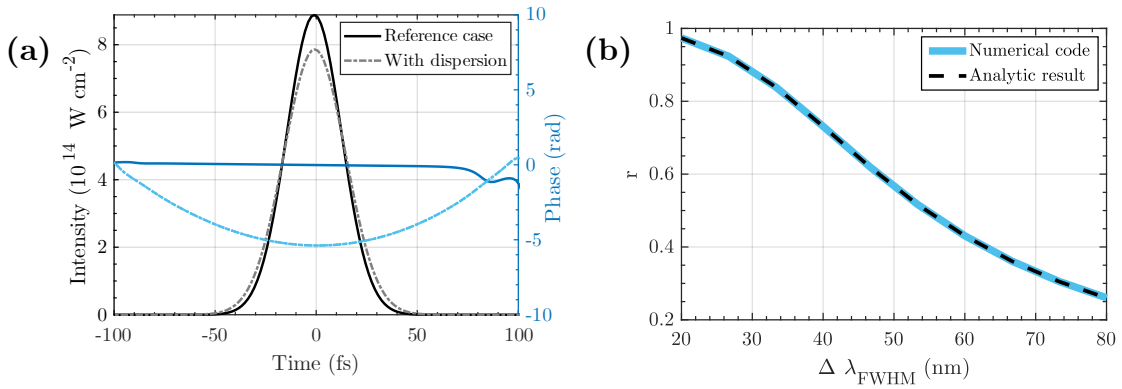

Figure 2. The effect of dispersion on the temporal intensity profile compared to a zero-dispersion reference case at $z = 20\,\text{mm}$. (a) shows the temporal intensity profile and corresponding temporal phase for $\Delta\lambda_{\text{FWHM}} = 30\,\text{nm}$. The reference is calculated assuming $n(\lambda) = n(\lambda_0)$. In (b), the calculated ratio r of the peak on-axis intensities obtained with dispersive and non-dispersive axicons is plotted as a function of the bandwidth of the incident pulse.

field of the beam, such as astigmatism. When small additional aberrations are modelled in the numerical code, the focal spot at $\delta = 0.0\,\text{mrad}$ can be kept close to the ideal Bessel shape, but as δ increases, the spot quality degrades faster than without the presence of these aberrations (see supplementary material). This behaviour may account for the discrepancy between the values of δ found in experiment and in simulation. Because the phase errors on the beam in the experimental setup could not be measured in this demonstration, the numerical code cannot exactly replicate the experimental conditions. Despite this limitation, the results presented in this section demonstrate the possibility of using the numerical code to predict the qualitative effect of different aberrations on the focal spot, which could be particularly useful when working with more complicated setups.

3. Study of chromatic effects through an axicon lens

To investigate the chromatic effects of a refractive axicon, the numerical code was run with inputs chosen to model an experiment recently performed on the RAL Astra-Gemini laser TA2 [10]. The laser was modelled as a bi-Gaussian pulse, with central wavelength $\lambda_0 = 805\,\text{nm}$, bandwidth $\Delta\lambda_{\text{FWHM}} = 30\,\text{nm}$ and incident peak intensity $I_0 = 6 \times 10^{11}\,\text{Wcm}^{-2}$. The laser spot size and propagation distance were scaled down by a factor of 10 to $\sigma = 2.54\,\text{mm}$ and $z = 20\,\text{mm}$ to enable adequate resolution without overloading the computer memory. This is equivalent to analysing the focus closer to the axicon tip than in the experimental setup.

The results of the simulation are shown in Figure 2. The reference case shown is for zero-dispersion through the refractive axicon, which is generated by setting $n(\lambda) = n(\lambda_0)$. As seen in Figure 2(a), it is found that, for the parameters used in this simulation, the effect of dispersion is to reduce the peak value to 89% of the reference value. The temporal phase is plotted on the same figure. The phase for the reference case is almost perfectly flat over the region of the pulse, suggesting that when dispersion is ignored the pulse is near diffraction-limited. Group delay dispersion is known to introduce a parabolic phase dependence [17], and this is what is observed for the dispersive case.

In order to gain further insight into the role of dispersion, we calculate the ratio of the peak axial intensity with and without dispersion (r) as a function of bandwidth of the incident pulse. Figure 2(b) plots this ratio for $z = 20\,\text{mm}$. As expected, the effect of dispersion increases with the

bandwidth, leading to greater reduction in peak intensity. For an incident beam with a Gaussian transverse profile, the analytic expression from Eq. 4 can also be used to investigate the effects of dispersion. Calculating the on-axis field at a fixed z-position for a number of wavelengths in the spectrum, and computing the inverse Fourier transform to the time domain (as in Eq. 3) generates the temporal intensity profile at that focus position. Again, the reference case was fixed with $n(\lambda) = n(\lambda_0)$. Figure 2(b) shows the excellent agreement between the numerical and analytic calculations, providing further validation of the numerical code.

4. Conclusion

We have developed a numerical code for applications in analysing the evolution of laser pulses through optical setups of relevance to laser wakefield accelerator experiments. The results of the numerical code were verified using comparisons to analytic expressions and to experiment. The application of the code to the investigation of chromatic effects through a refractive axicon revealed that dispersion is expected to have only a minor effect on the on-axis intensity for a bandwidth of 30 nm.

The calculations presented above do not include nonlinear effects. In propagating through a medium, a pulse accumulates nonlinear phase $\phi_{\mathrm{NL}} = \int kn_2 I(z)dz$ where n_2 is the nonlinear refractive index. The nonlinear phase leads to self focusing and self phase modulation, the latter of which further increases the pulse bandwidth. To avoid these problems it is therefore usual to seek to keep $\phi_{\mathrm{NL}} < 1$. However, for the parameters considered here, the thickest part of the axicon introduces $\phi_{\mathrm{NL}} \approx 4$. Additional efforts are currently ongoing to incorporate these nonlinear effects into the code.

We note that the problems caused by dispersion and nonlinear phase could be eliminated by using a reflective rather than transmissive optic. Other optics which may be of interest for channel formation, such as kinoforms, axilenses and axiparabolas, may also be modelled using the numerical code for future investigations. The results of these simulations could be used as input to other codes, such as particle-in-cell or plasma hydrodynamic codes, to model the resulting formation and evolution of the plasma channel.

Acknowledgments

This work was supported by the UK Science and Technology Facilities Council (STFC UK) [grant numbers ST/P002048/1, ST/N504233/1, ST/R505006/1, ST/S505833/1]. This material is based upon work supported by the Air Force Office of Scientific Research under award number FA9550-18-1-7005. This work was supported by the European Union's Horizon 2020 research and innovation programme under Grant Agreement No. 653782 and Grant Agreement No. 730871.

References

[1] Albert F and Thomas A G R 2016 *Plasma Physics and Controlled Fusion* **58** 103001

[2] Li X, Mosnier A and Nghiem P A P 2018 *Nucl. Instrum. Methods Phys. Res. A* **909** 49 – 53 ISSN 0168-9002 3rd European Advanced Accelerator Concepts workshop (EAAC2017)

[3] Sun G Z, Ott E, Lee Y and Guzdar P 1987 *The Physics of Fluids* **30** 526–532

[4] Esarey E, Schroeder C B and Leemans W P 2009 *Rev. Mod. Phys.* **81**(3) 1229–1285

[5] Spence D J and Hooker S M 2000 *Phys. Rev. E* **63** 015401

[6] Butler A, Spence D J and Hooker S M 2002 *Phys. Rev. Lett.* **89** 185003

[7] Gonsalves A J, Nakamura K, Daniels J, Benedetti C, Pieronek C, de Raadt T C H, Steinke S, Bin J H, Bulanov S S, van Tilborg J, Geddes C G R, Schroeder C B, Tóth C, Esarey E, Swanson K, Fan-Chiang L, Bagdasarov G, Bobrova N, Gasilov V, Korn G, Sasorov P and Leemans W P 2019 *Phys. Rev. Lett.* **122**(8) 084801

[8] Durfee C G and Milchberg H M 1993 *Phys. Rev. Lett.* **71**(15) 2409–2412

[9] Shalloo R J, Arran C, Corner L, Holloway J, Jonnerby J, Walczak R, Milchberg H M and Hooker S M 2018 *Phys. Rev. E* **97**(5) 053203

[10] Shalloo R J, Arran C, Picksley A, von Boetticher A, Corner L, Holloway J, Hine G, Jonnerby J, Milchberg H M, Thornton C, Walczak R and Hooker S M 2019 *Phys. Rev. Accel. Beams* **22**(4) 041302

[11] McLeod J H 1954 *J. Opt. Soc. Am.* **44** 592–597

[12] Davidson N, Friesem A A and Hasman E 1991 *Opt. Lett.* **16** 523–525

[13] Smartsev S, Caizergues C, Oubrerie K, Gautier J, Goddet J P, Tafzi A, Phuoc K T, Malka V and Thaury C 2019 *Opt. Lett.* **44** 3414–3417

[14] Goodman J W 2005 *Introduction to Fourier Optics* (Roberts & Company Publishers)

[15] Wang Y, Yan S, Friberg A T, Kuebel D and Visser T D 2017 *J. Opt. Soc. Am. A* **34** 1201–1211

[16] Refractive Index Information `https://refractiveindex.info` [Accessed 24-January-2020]

[17] Hooker S M and Webb C 2010 *Laser Physics* (Oxford University Press)